# Free-Flight Investigation of the Aerodynamic Characteristics of a Cone at High Mach Numbers

C. J. WELSH,* G. L. WINCHENBACH,† AND A. N. MADAGAN‡
*ARO Inc., Arnold Air Force Station, Tenn.*

**A 1000-ft hypervelocity range was used to obtain the free-flight static and dynamic stability and drag data presented for a 10° semiangle cone. Measurements indicate that the damping-in-pitch derivatives for the cone increase appreciably with increasing Mach number between $M = 8$ and 16 at a Reynolds number (based on model length and freestream conditions) of about $0.4 \times 10^6$. Further, $C_{m\alpha}$ for the cone decreases significantly as the nose-radius to base-radius ratio of the cone is increased up to 0.1 for amplitudes greater than about 5°. Comparisons of the range stability data with wind-tunnel data (involving sting-supported models) obtained in different test facilities indicate that appreciable differences in $C_{m\alpha}$ and $(C_{mq} + C_{m\dot{\alpha}})$ exist in some cases.**

## Nomenclature§

| | | |
|---|---|---|
| $C_{D0}$ | = | drag coefficient at zero angle of attack |
| $C_{mq} + C_{m\dot{\alpha}}$ | = | damping-in-pitch derivatives, $[\partial C_m/\partial q(d/2V)] + [\partial C_m/\partial \dot{\alpha}(d/2V)]$ |
| $C_{m\alpha}$ | = | pitching-moment derivative |
| $C_{N\alpha}$ | = | normal-force derivative |
| $C_p$ | = | pressure coefficient |
| $cg$ | = | position of the center of gravity, percentage of model length from the nose |
| $cp$ | = | position of the center of pressure, percentage of model length from the nose |
| $d$ | = | model diameter, and moment reference length |
| $L_1, L_2$ | = | define lengths of flight intervals used in reducing data |
| $l$ | = | model length |
| $M$ | = | Mach number |
| $R_B$ | = | base radius of model |
| $Re_l$ | = | Reynolds number based on freestream conditions and model length |
| $R_N$ | = | nose radius of model |
| $V$ | = | model velocity |
| $\alpha_{\text{mean}}$ | = | mean angle of attack |
| $\alpha_0$ | = | initial angle of attack |
| $\beta, \alpha$ | = | components of the complex yaw angle |
| $\delta_l$ | = | local body slope with respect to the freestream velocity |
| $\bar{\delta}$ | = | $\left[\left(\frac{1}{L_2 - L_1}\right)\int_{L_1}^{L_2} (\beta^2 + \alpha^2)dx\right]^{1/2}$ |
| $\omega$ | = | angular frequency |

Presented as Paper 69-133 at the AIAA 7th Aerospace Sciences Meeting, New York, January 20–22, 1969; submitted February 3, 1969; revision received July 17, 1969. The authors wish to acknowledge the contribution of C. J. Stalmach for the Ling-Temco-Vought data and the contributions of L. K. Ward Jr. and B. L. Uselton for the AEDC wind-tunnel data. The research reported in this paper was sponsored by the Arnold Engineering Development Center (AEDC), Air Force Systems Command (AFSC), under Contract F40600-69-C-0001 with ARO Inc.

* Supervisor, External Ballistics Section, Aeroballistics Branch, von Kármán Gas Dynamics Facility. Associate Member AIAA.

† Project Engineer, External Ballistics Section, Aeroballistics Branch, von Kármán Gas Dynamics Facility. Associate Member AIAA.

‡ Project Engineer, External Ballistics Section, Aeroballistics Branch, von Kármán Gas Dynamics Facility; now with the Martin-Marietta Corporation, Orlando, Fla. Associate Member AIAA.

§ Reference area for all coefficients and derivatives is based on model diameter.

## I. Introduction

AERODYNAMIC characteristics of slender cones have received a considerable amount of attention from various investigators in recent years; however, only a very limited amount of experimental stability data for cones at high Mach numbers has been published. Concern has existed regarding some of these stability measurements made in the past because of apparent inconsistencies in the test results (see, for example, the comments of Hobbs in Ref. 1). Concern has also existed regarding an apparent stability problem detected in previous cone testing, specifically, damping derivatives decreasing to near zero with increasing Mach numbers, as has been observed in wind-tunnel tests of a 10° semiangle cone at Mach numbers between 10 and 20.

In consideration of the factors noted in the previous comments, it was felt that some free-flight stability measurements for cones could be of particular significance. Hence, a series of free-flight tests has been made in which the aerodynamic characteristics of a 10° semiangle cone have been investigated at Mach numbers from 6 to 16 for Reynolds numbers, based on model lengths and freestream conditions, from $0.2 \times 10^6$ to $11 \times 10^6$. The tests were conducted in the von Kármán Gas Dynamics Facility (VKF), Arnold Engineering Development Center (AEDC) 1000-ft Hypervelocity Range G.

The purpose of this paper is to present the results of this investigation, including both stability and drag data. Further, the range stability derivatives are compared with analytically predicted values and with wind-tunnel data obtained in different facilities.

## II. Apparatus

### Range

The VKF Range G consists of a 10-ft-diam, 1000-ft-long tank contained within an underground tunnel. It is a variable density aerodynamic range and has an 840-ft instrumented length that includes 43 equally spaced, dual-plane shadowgraph stations. The shadowgraph system permits determining the angular orientation and position of most test configurations to within approximately ±0.25° and ±0.002 ft, respectively, at each station. A chronograph system measures intervals of flight time to within $\pm 2 \times 10^{-7}$ sec. The range vacuum pumping system provides range pressures from one atmosphere down to about 15 μHg. The 15-μHg pressure level corresponds to an equivalent altitude of approximately 250,000 ft. The nominal operating

**Table 1 Maximum probable errors, %**

| $C_{D0}$ | $C_{m\alpha}$ | $C_{mq} + C_{m\dot{\alpha}}$ | $C_{N\alpha}$ | $cp$ |
|---|---|---|---|---|
| ±4 | ±3 | ±10 | ±5 | ±0.3 |

temperature of the range is 76°F. The launcher normally used with the range is a two-stage, light-gas gun having a 2.5-in.-diam launch tube.

### Models and Sabots

The configuration investigated was a 10° semiangle cone, and the models used had a nominal base diameter of either 1 or 1.75 in. and a designed nose-to-base-radius ratio ($R_N/R_B$) of either 0.035 or 0.07. The models were constructed basically of either aluminum or steel; however, models designed for testing at the higher heating conditions were equipped with copper nose tips.

The sabots used in the test program were of a conventional four-component design and were aerodynamically separated from the models in the blast tank portion of the range. All models were launched in an uncanted orientation relative to the sabot, and the initial angular disturbances to the models were those arising from muzzle effects and from the model-sabot separation process.

## III. Data Reduction

The aerodynamic data of the present test program were reduced consistently with data reduction methods discussed in Ref. 2. A discussion of the effects of small roll rates on the yawing motion of statically stable bodies and the limitations associated with certain simplified data analysis procedures can be found in Ref. 3. The estimated maximum probable errors in the data presented in this paper are listed in Table 1.

## IV. Ballistic Range Tests

### Dynamic Stability Derivatives

Measured $C_{mq} + C_{m\dot{\alpha}}$ values as a function of Reynolds number, for Mach numbers near 6.5, are shown in Fig. 1. The level and trend of the damping values for a laminar boundary layer ($Re_l < 4.5 \times 10^6$) are well defined. For the higher Reynolds number shots ($Re_l > 4.5 \times 10^6$) the location of transition is in the region of the model base. The increased spread in the measurements at the highest Reynolds numbers is believed to be related to fluctuations in the location of transition and is indicative of the increased difficulty in obtaining consistent damping measurements for this test condition. The damping levels predicted by the shock expansion method[4] and the unsteady flowfield method[5] are also shown in Fig. 1, and both are lower than that indicated by the range data.

Damping derivatives as a function of Mach number, for $Re_l \approx 0.4 \times 10^6$, are presented in Fig. 2. Except for the two low data points (square symbols) at $M \approx 15$, the measurements are quite consistent and indicate a marked increase in damping with increasing Mach number. The circular symbols represent shots for which the models experienced nonplanar motion patterns, but these patterns were comparable to model motion in one-degree-of-freedom wind-tunnel tests; that is, the model on these shots experienced a near zero transverse velocity component (component normal to the angle-of-attack plane) at its maximum amplitude. The other three shots (square symbols) had combinations of a rolling velocity and a wider elliptic motion pattern such that the model would tend to have a larger transverse velocity component at its maximum amplitude. The differences in the measured damping levels indicated at $M \leftrightarrows 15$

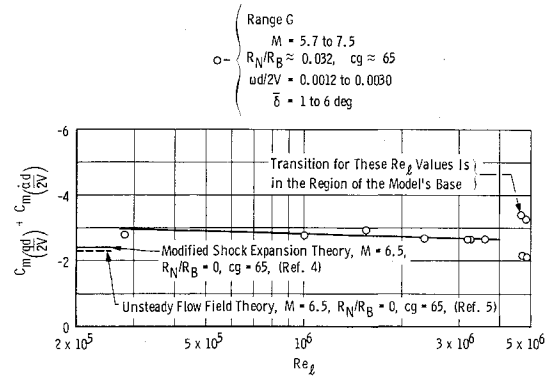


**Fig. 1 Damping-in-pitch derivatives for $M \approx 6.5$.**

are believed to be real, and although the problem is not understood, the measurements suggest that the damping derivatives at higher Mach numbers may have some dependence on the type of motion pattern experienced by the model. Within the band of amplitudes of the present measurements ($\bar{\delta} = 2.5°–12°$), no amplitude effect on damping was detected.

The two theoretical curves,[4,5] shown in Fig. 2, indicate a small increase in the damping derivatives with increasing Mach number, but this increase is not as large as that indicated by the experimental measurements. In view of the larger increase in the experimental damping values with Mach number than was expected, particular care was exercised in examining different factors that could have possibly affected the data; however, nothing has been found to invalidate the experimental measurements.

One potential error source that was considered in some detail was the effect of the geometry of the model nose changing during the flight owing to aerodynamic heating. At the higher Mach numbers, the shadowgrams of the model indicated that a slight change in nose bluntness occurred during flight, and in the worst case the $R_N/R_B$ ratio increased to about 0.07 at the downrange end of the range. It has been noted in previous range testing that a copper nose tip at high heating conditions appears to melt, and a portion of the tip material is redistributed along the nose of the model immediately aft of the tip. In fact, it is questionable whether any mass is actually lost from copper nose models. Hence, any nose effect existing in the present measurements is believed to be related to the small change in nose geometry rather than to actual material ablation.

In an attempt to assess the effect of the small changes in nose geometry on the damping measurements, a series of shots was analyzed independently over the first half and over the second half of their flights. It follows that if nose

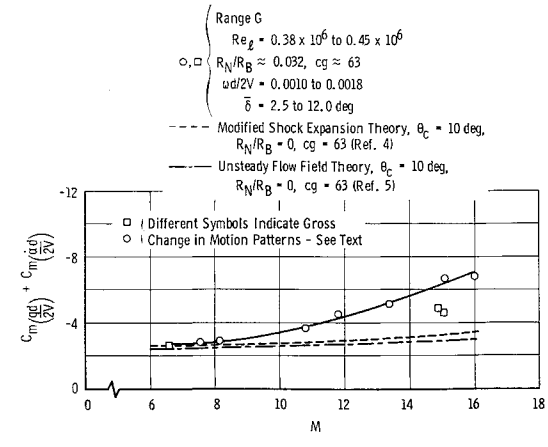


**Fig. 2 Damping-in-pitch derivatives for $Re_l \approx 0.4 \times 10^6$.**

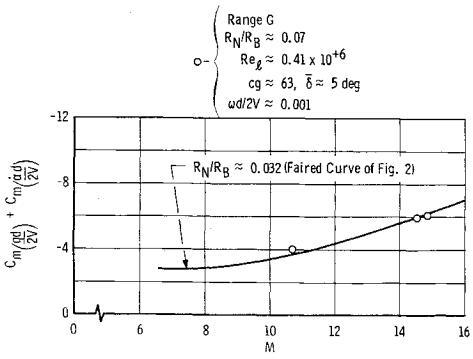


**Fig. 3 Damping-in-pitch derivatives for different nose bluntness ratios.**

geometry effects were large, they would be reflected in damping values reduced in this manner. The results of this analysis indicated no consistent differences in the reduced damping values obtained for the first and second portions of the individual flights. That is, the damping values obtained during the first portion of these flights were neither consistently higher nor lower than those for the second portion. Furthermore, the differences in the damping values computed for the first and second portions of the individual shots were always small relative to the experimentally observed increase in damping at the higher Mach numbers. It is also significant that, for shots at Mach numbers up through $M \approx 11$, no nose shape change was detectable; however, the data point at $M \approx 11$ is consistent with the trend established by the higher Mach number shots in indicating increased damping with Mach number.

Further indication of the negligible effect of nose geometry changes on the dynamic stability derivatives was obtained from the damping measurements for three shots using models with a larger initial bluntness ratio ($R_N/R_B \approx 0.07$), presented in Fig. 3. Nose shape changes for these models would necessarily be smaller than those for models with the sharper tip; however, these shots also show a similar trend of increasing damping with increasing Mach number. Also shown in Fig. 3 is a curve representing the data given in Fig. 2 for $(R_N/R_B) \approx 0.032$. It is of interest that the measurements do not indicate any significant effect of bluntness on damping, within the small bluntness change of the present tests.

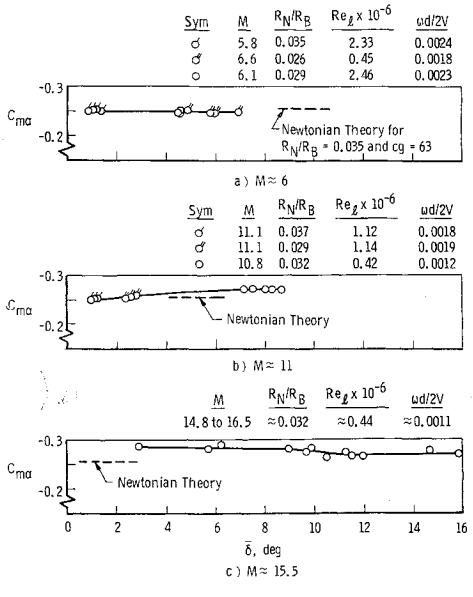


**Fig. 4 Static stability parameter as a function of amplitude for $R_N/R_B \approx 0.032$ (data adjusted to $cg = 63$).**

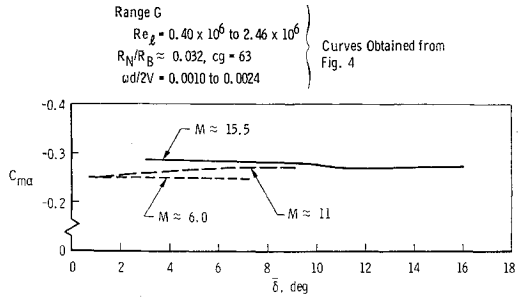


**Fig. 5 Comparison of $C_{m\alpha}$ variations for three Mach numbers.**

### Static Stability Derivatives

In examining the $C_{m\alpha}$ data of the test program, it became apparent that $C_{m\alpha}$ was more sensitive to amplitude for some test conditions than had been anticipated. Hence, the amount of available data was not sufficient to define well the effects of amplitude on $C_{m\alpha}$ in some cases. However, certain variations of $C_{m\alpha}$ with amplitude are indicated in the limited number of range measurements, and these are discussed. In this paper, adjustments of $C_{m\alpha}$ data (either range or wind-tunnel data) to another moment reference position were made using a $C_{N\alpha}$ value of 1.91.

Measured variations of $C_{m\alpha}$ with amplitude for $R_N/R_B \approx 0.032$ are shown in Fig. 4 for Mach numbers near 6, 11, and 15.5. A sectional curve fitting procedure wherein the equation of motion is fitted to the motion data of different portions of a flight was used in some cases in reducing the $C_{m\alpha}$ data. The sectional fitting procedure is an aid in identifying amplitude effects in $C_{m\alpha}$ data for some test conditions.

Within the band of $M$, $R_N/R_B$, and $Re_l$ for the shots involved, the measurements at $M \approx 6$ (Fig. 4a) indicate a near constant $C_{m\alpha}$ for mean amplitudes up to about 7°; whereas, at $M \approx 11$ (Fig. 4b) a slight increase in $C_{m\alpha}$ with amplitude is indicated. It is believed that the variation in $C_{m\alpha}$ with amplitude, shown in Fig. 4b (note the $C_{m\alpha}$ variations for individual shots), is related to amplitude differences rather than to the differences in Reynolds number listed in Fig. 4b for the shots involved. The $C_{m\alpha}$ values presented in Fig. 4c for $M \approx 15.5$ were measured over the first one-third portion of the range length because of the higher nose heating conditions associated with these shots, and any effects of possible nose geometry changes on the presented $C_{m\alpha}$ values are believed to be negligibly small. In general, the variation of $C_{m\alpha}$ was small for mean amplitudes up to about 16°; however, the data in Fig. 4c suggest an apparent slight shift in magnitude in the amplitude region near $\bar{\delta} = 10.5°$ (near the cone semiangle). Also shown in Fig. 4 are the Newtonian predicted levels of $C_{m\alpha}$ which are in reasonable agreement with the present measurements. It should be noted that the Newtonian theory as used in this paper is the unmodified Newtonian theory ($Cp = 2 \sin^2\delta_l$).

The faired $C_{m\alpha}$ curves of Fig. 4 are replotted in Fig. 5 and indicate that $C_{m\alpha}$ increases slightly with Mach number for mean amplitudes between about 3° and 7°.

Measured variations of $C_{m\alpha}$ as a function of $\bar{\delta}$ are shown in Fig. 6 for cones having larger bluntness ratios. The data for $R_N/R_B \approx 0.1$, shown in Fig. 6c, were obtained in a previous Range G test program.[6] For comparison purposes, the faired $C_{m\alpha}$ curves of Fig. 6 are replotted in Fig. 7. Also shown in Fig. 7 is the faired $C_{m\alpha}$ curve of Fig. 4c for $R_N/R_B \approx 0.032$ and $M \approx 15.5$. The measurements indicate an appreciable decrease in $C_{m\alpha}$ for an increase in $R_N/R_B$ from 0.032 to 0.07 at $M \approx 15$. It is of significance that, at this Mach number, the limited amount of data indicates that the difference obtained in $C_{m\alpha}$ for the two values of $(R_N/R_B)$ diminishes at the lower amplitudes and suggests the possibility that $C_{m\alpha}$ may be higher for the blunter cone at values

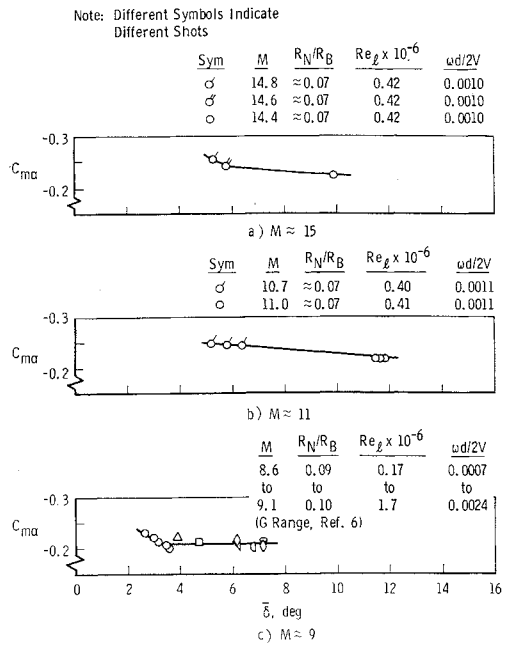


**Fig. 6 Static stability parameter as a function of amplitude for $(R_N/R_B)$ = 0.07 and 0.1 (data adjusted to $cg$ = 63).**

of $\bar{\delta}$ near zero. At $M \approx 11$, a $C_{m\alpha}$ level is observed similar to that at $M \approx 15$, indicating that any Mach number effect on $C_{m\alpha}$ in this amplitude and Mach number range is small. The marked increase in $C_{m\alpha}(R_N/R_B = 0.07)$ noted for the lower amplitudes in the $M \approx 15$ data is not evident in the $M \approx 11$ data at comparable amplitudes. The $M \approx 9$ data for $(R_N/R_B) = 0.1$ (from Ref. 6) show a further decrease in $C_{m\alpha}$ below the level of the data for $M \approx 11$ and $M \approx 15$. This lower level in $C_{m\alpha}$ is believed to be associated primarily with the further increase in bluntness rather than with the Mach number difference because of the small Mach number effect noted previously in the data at $M \approx 15$ and $M \approx 11$. A marked increase in $C_{m\alpha}$ similar to that obtained at $M \approx 15$ is observed in the $M \approx 9$ data for amplitudes less than 4°. It appears from the experimental data of this figure that the amplitude associated with the increase in $C_{m\alpha}$, observed at smaller amplitudes, is Mach number dependent. Unfortunately, the absence of sufficient low-amplitude data at $M \approx 11$ precludes further confirmation of this observation. Within the assumption that any Mach number effect on $C_{m\alpha}$ is small, the present measurements indicate, for amplitudes in the range between 6° and 10°, that $C_{m\alpha}$ decreases with increasing bluntness for $R_N/R_B$ values up to at least 0.1.

Values of $C_{m\alpha}$ obtained, for $\bar{\delta}$ = 7°, from the curves of Fig. 7 and the level of $C_{m\alpha}$ obtained in a free-flight wind-tunnel test at AEDC are shown in Fig. 8 as a function of bluntness ratio. Also shown in Fig. 8 are the variations of $C_{m\alpha}$ with bluntness ratio that are predicted by the Newtonian and

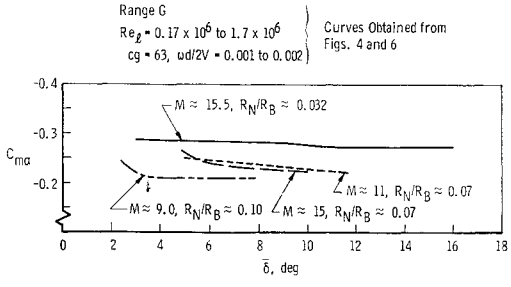


**Fig. 7 Comparison of $C_{m\alpha}$ values for different bluntness ratios.**

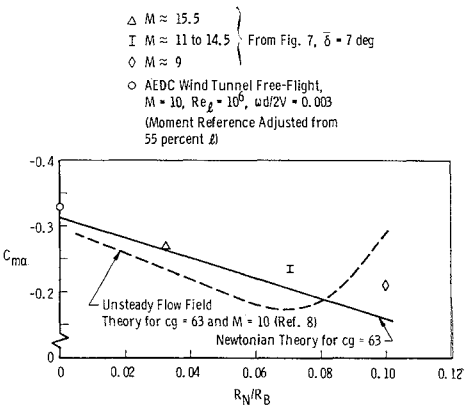


**Fig. 8 Variation of $C_{m\alpha}$ with bluntness ratio for $\bar{\delta}$ = 7° (moment reference at 63% $l$).**

the unsteady flowfield theories which are for amplitudes near zero. The general trends of the theoretical curves are consistent with the decrease in $C_{m\alpha}$ indicated in the free-flight measurements for the small range of nose bluntness ratio, at $\bar{\delta}$ = 7°. However, as noted previously, the present measurements for bluntness ratios of 0.07 and greater (see Fig. 7) suggest that at amplitudes near zero a nose bluntness may result in a greater $C_{m\alpha}$ than for a pointed cone. Further experimental evidence of this effect can be obtained from data presented in Ref. 7. The tests of Ref. 7 were at $M$ = 14 and at amplitudes less than 2.8°, and the measured $C_{m\alpha}$ for a 10° semiangle cone $(R_N/R_B = 0.1)$ was appreciably larger than the $C_{m\alpha}$ for a pointed cone; it should be noted that this comment is valid for $C_{m\alpha}$ measurements of Ref. 7 referenced to a common pivot axis position expressed as a percentage of actual model length from the nose.

In Fig. 9, $C_{m\alpha}$ values (adjusted to $cg$ = 65) are shown as a function of Reynolds number. These measurements are for Mach numbers near 6. An examination of schlieren photographs indicated that the lowest data point of the group of data points near $Re_l = 4.8 \times 10^6$ corresponded to a shot that had a laminar boundary layer over the complete length of the model. This shot also had the lowest amplitude, $\bar{\delta}$ = 0.7° Schlieren photographs for other shots of this group (higher amplitudes) indicate that the location of transition was near the base of the model. Hence, the faired curve in Fig. 9 is believed to be representative of the variation of $C_{m\alpha}$ with Reynolds number for a cone having a laminar boundary layer. The limited measurements available at the higher Reynolds numbers indicate that $C_{m\alpha}$ increases slightly as transition moves onto the cone.

### Normal-Force Derivative

The variation of $C_{N\alpha}$ with amplitude, for $M \approx 6$ and over a Reynolds number range from $0.2 \times 10^6$ to $5 \times 10^6$, are shown in Fig. 10. The $C_{N\alpha}$ measurements (for $R_N/R_B \approx 0.032$) are nearly constant for $\bar{\delta}$ up to 6°. These data indicate that at $M$ = 6 the effect of Reynolds number on $C_{N\alpha}$ within the above $Re_l$ range is not significant. The $C_{N\alpha}$ level pre-

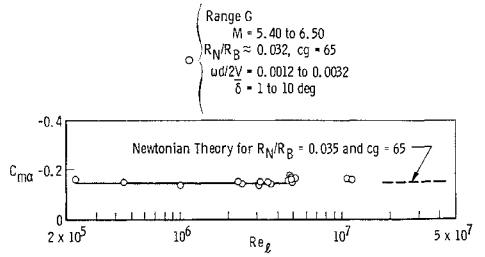


**Fig. 9 Variation of $C_{m\alpha}$ with $Re_l$ for $M \approx 6$.**

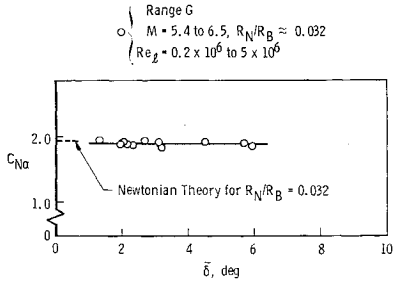


**Fig. 10 Variation of the normal force derivatives with amplitude ($M \approx 6$).**

dicted by the Newtonian theory is also shown in Fig. 10 and is in good agreement with the present measurements.

Variations of $C_{N\alpha}$ with amplitude, for $Re_l \approx 0.4 \times 10^6$ and for Mach numbers from 6 to 16, are shown in Fig. 11. The measurements shown in Fig. 11a indicate that, again, the $C_{N\alpha}$ values (for $R_N/R_B \approx 0.032$) are nearly constant for $\bar{\delta}$ up to at least 18°. Further, the measurements indicate that $C_{N\alpha}$ tends to be insensitive to Mach number. The faired $C_{N\alpha}$ curve of Fig. 11a is replotted in Fig. 11b. Also shown in Fig. 11b are measurements for $R_N/R_B \approx 0.07$ and for $Re_l \approx 5 \times 10^6$. The limited number of measurements does not indicate any significant effects of either Reynolds number or of small nose bluntness on $C_{N\alpha}$. The $C_{N\alpha}$ levels predicted by the Newtonian theory, for $R_N/R_B = 0.032$ and 0.07, are also shown in Fig. 11 and are in good agreement with the present measurements.

### Center of Pressure

The variations of $cp$ with Reynolds number, amplitude, and Mach number are shown in Fig. 12. The measurements in Fig. 12a, for $M \approx 6$ and for $\bar{\delta}$ up to about 6°, indicate that $cp$ (for $R_N/R_B \approx 0.032$) tends to be insensitive to Reynolds number if the model has a laminar boundary layer. As stated previously, for $Re_l \approx 4.8 \times 10^6$, the location of transition for $M \approx 6$ is near the base of the model. The lowest data point (more forward $cp$) in the group of data points at Reynolds numbers near $4.8 \times 10^6$, corresponds to the shot noted in the discussion of the $C_{m\alpha}$ data of Fig. 9 and has the lowest amplitude, $\bar{\delta} = 0.7°$. Hence, this group of data points would suggest that the $cp$ moves slightly rearward as transition moves onto the cone.

The $cp$ measurements for $M \approx 15 (R_N/R_B \approx 0.032, Re_l \approx 0.4 \times 10^6)$ are plotted as a function of amplitude in Fig. 12b. These data do not indicate any significant effect of amplitude on the $cp$.

Measurements in Fig. 12c, for $Re_l \approx 0.4 \times 10^6$ and for mean amplitudes from 5° to 12°, indicate that $cp$ (for $R_N/R_B$

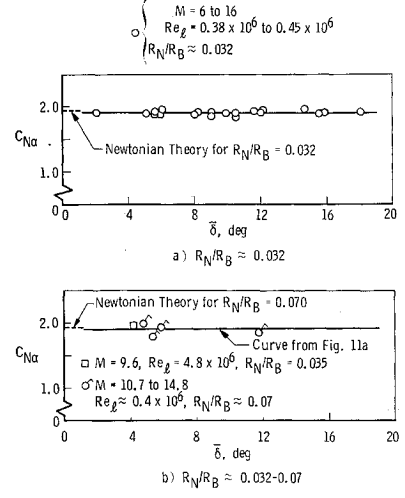


**Fig. 11 Variation of the normal force derivative with amplitude ($M = 6$-16).**

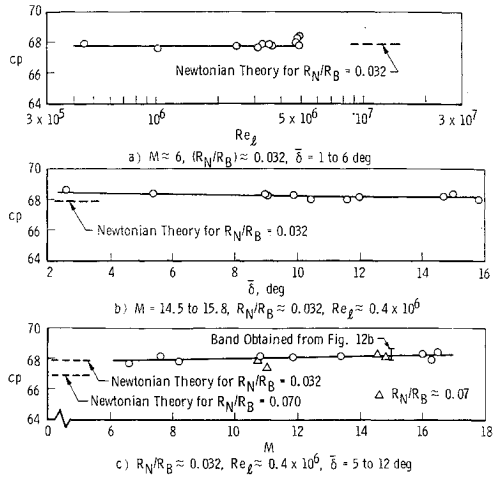


**Fig. 12 Center of pressure as a function of Reynolds number, amplitude, and Mach number.**

$\approx 0.032$) moves slightly rearward with increasing Mach number. The $cp$ measurements for $R_N/R_B \approx 0.07$, also shown in Fig. 12c, are in general agreement with the $cp$ values for the sharper cone; the lower data point (triangular symbol) at $M \approx 11$ is believed to be lower because of the higher amplitude ($\bar{\delta} \approx 11.5°$) of this shot in combination with the larger bluntness ratio.

The levels of $cp$ predicted by the Newtonian theory are also shown in Fig. 12 and are in reasonable agreement with the present measurements.

### Drag Coefficient

Drag coefficient $C_{D0}$ is presented as a function of Mach number in Fig. 13 for $Re_l \approx 0.4 \times 10^6$. Measurements indicate that $C_{D0}$, for $R_N/R_B \approx 0.032$, decreases with increasing Mach number. Additional drag measurements shown in Fig. 13 for bluntness ratios from 0.02 to 0.07 indicate that $C_{D0}$ tends to be insensitive to small changes in nose bluntness.

Some $C_{D0}$ measurements, for $M \approx 6$, are shown as a function of Reynolds number in Fig. 14. The lowest data point in the group of data points near $Re_l = 4.8 \times 10^6$ corresponds to the same shot noted in the discussion of the $C_{m\alpha}$ data of Fig. 9. It was noted then that this shot had the minimum amplitude, $\bar{\delta} = 0.7°$, and that the schlieren photograph for this shot indicated that the model had a laminar boundary layer over its entire length. Hence, the faired curve in Fig. 14 is believed representative of the $C_{D0}$ variation for the case of the cone having a laminar boundary layer.

The variation of $C_{D0}$ as transition moves onto the cone is not defined adequately in the present tests, partially because of the sensitiveness of the location of transition with small amplitude changes; however, the measurements at the higher Reynolds numbers indicate an appreciable increase in $C_{D0}$ as transition moves onto the cone.

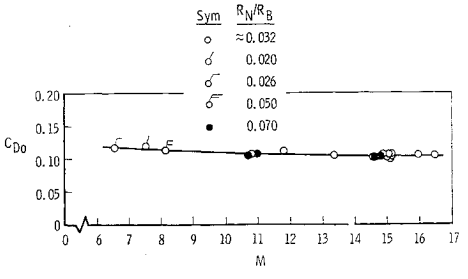


**Fig. 13 Drag coefficient as a function of Mach number ($Re_l \approx 0.4 \times 10^6$).**

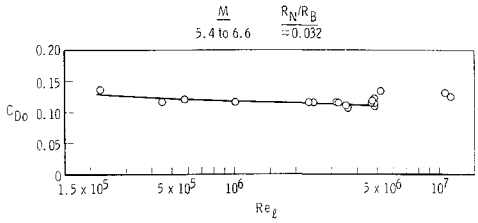


**Fig. 14 Variation of zero-lift drag coefficient with Reynolds number ($M \approx 6$).**

## V. Comparison of Range Data with Wind-Tunnel Data

Comparisons of the present range measurements with wind-tunnel data are shown in Figs. 15–19. The faired $C_{m\alpha}$ curve ($M \approx 6$) of Fig. 9, corresponding to a condition of a laminar boundary layer, is replotted in Fig. 15. Also shown in Fig. 15 are $C_{m\alpha}$ measurements for a sting-supported 10° semiangle cone obtained at the Jet Propulsion Laboratory (JPL)[9] for similar test conditions. The JPL measurements have been adjusted to a moment reference at 65% of the cone length from the nose. The significance of this data comparison is related to the different trends exhibited in the two sets of data. The JPL measurements increase appreciably with decreasing Reynolds number, whereas the range measurements are nearly constant. The difference in absolute magnitude of $C_{m\alpha}$ between the two sets of measurements is of no concern because of the different nose bluntness ratios (indicated in Fig. 15) that are involved.

In Fig. 16, a comparison is made between the range damping data (faired curve replotted from Fig. 1) for $M \approx 6$ and damping measurements obtained in the JPL tests.[9] The range measurements indicate somewhat more damping than measured in the JPL tests. In consideration of previous comments regarding nose bluntness effects on damping, the effect of the small difference in $R_N/R_B$ existing in the data shown in Fig. 16 would be expected to be negligibly small.

A comparison of the range damping level at $M = 10$ with wind-tunnel data obtained at AEDC at the same Mach number and over a range of *cg* position is shown in Fig. 17. Two theoretical curves are also shown in Fig. 17 to indicate the predicted trend of the damping derivatives with *cg* position. The wind-tunnel data include results from free-flight models (at AEDC) and both gas-bearing-mounted and flexure-mounted, sting-supported models (AEDC), all tested in the same wind tunnel at similar flow conditions. Also included are measurements (using a flexure pivot), taken from Ref. 10, made at a single *cg* position and at three different frequencies.

Both range and tunnel free-flight dynamic stability measurements tend to be larger than the measurements for the sting-mounted models. These free-flight measurements in the range and wind tunnel tend to be consistent with one

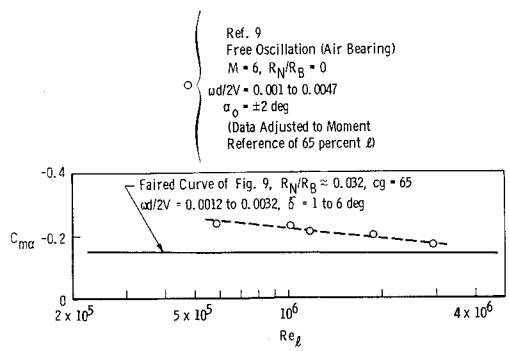


**Fig. 15 Comparison of range and tunnel $C_{m\alpha}$ data at $M \approx 6$.**

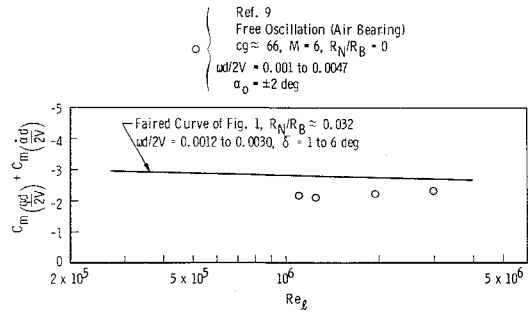


**Fig. 16 Comparison of range and tunnel damping data at $M \approx 6$.**

another, although there is a difference in Reynolds numbers between the two sets of measurements ($Re_l \backsimeq 0.4 \times 10^6$ and $10^6$ for the range and tunnel tests, respectively).

The Ref. 10 data, at a $Re_l$ comparable to the range data, indicate a frequency effect on damping, as shown in Fig. 17. It should be noted that apparent frequency effects on dynamic stability measurements have been observed in other tunnel tests. The portion of the Ref. 10 measurements which were obtained at frequencies comparable to the free-flight data in Fig. 17 indicate considerably less damping than the free-flight data. The portion of the Ref. 10 data band which appears to agree, in general, with the magnitude of the free-flight data in the figure is for an appreciably higher oscillation frequency than that corresponding to the free-flight data. On this basis, he frequency effect indicated in the data of Ref. 10 appears to be inconsistent with the range and tunnel free-flight measurements.

In Fig. 18, a comparison is made of the range $C_{m\alpha}$ data and wind-tunnel data (involving sting-supported models) for high Mach numbers obtained from different facilities [Ref. 11 and AEDC (VKF) and Ling-Temco-Vought, Dallas, Tex.] The solid curve in Fig. 18 corresponds to range $C_{m\alpha}$ values obtained from the curves of Fig. 5 at $\bar{\delta} = 5°$. The $\bar{\delta}$ of 5° is a reasonable mean value of the amplitude band involved in the different sets of data shown in Fig. 18. The range $C_{m\alpha}$ curve (Fig. 18) is representative of a Reynolds number comparable to the different sets of wind-tunnel data shown in Fig. 18; however, the range measurement at $M \approx 9.6$ and $Re_l = 4.8 \times 10^6$ shown in Fig. 18 fails to indicate any significant effect of Reynolds number on $C_{m\alpha}$. From considerations of the nose bluntness differences noted in Fig. 18, the tunnel measurements would be expected to be higher

| Sym | $R_N/R_B$ | $Re_\ell$ | ωd/2V | Amplitude, deg | Method Data Obtained | Facility (AEDC) |
|---|---|---|---|---|---|---|
| ● | ≈0.035 | ≈0.4 x $10^6$ | ≈0.0012 | $\bar{\delta} \approx 5$ | Free-Flight Range | Range G |
| ▲ | 0 | ≈$10^6$ | 0.003 | $\bar{\delta} \approx 7$ | Free-Flight Tunnel | Tunnel C |
| ▨ | 0 | ≈$10^6$ | 0.002 to 0.004 | $\alpha_0$ = 2 to 8 | Includes Both Free and Forced Oscillation, and Gas Bearing and Flexure Pivot Data | Tunnel C |
| I | 0.017 | 0.36 x $10^6$ | 0.0024 to 0.0125 | $\alpha_{mean}$ = 1.5 | Free Oscillation (Flexure Pivot) Ref. 10 | Tunnel C |

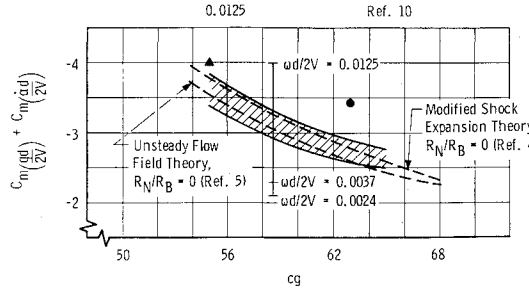


**Fig. 17 Comparison of range and tunnel damping data at $M = 10$.**

| Sym | $R_N/R_B$ | $Re_\ell$ | $\omega d/2V$ | Amplitude deg | Facility | Method Data Obtained |
|---|---|---|---|---|---|---|
| ○ | 0.035 | $4.79 \times 10^6$ | 0.0024 | $\bar{\delta} = 4.2$ | VKF | Free-Flight (Moment Reference Adjusted from 65 percent $\ell$) |
| □ | 0 | $\approx 0.165 \times 10^6$ | 0.0115 | $\alpha_0 = 1.75$ | LTV | Tunnel-Free Oscillation (Moment Reference Adjusted from 54.8 percent $\ell$) |
| ⌶ | 0 | $0.45 \times 10^6$ to $0.50 \times 10^6$ | 0.0043 | $\alpha_0 = 3$ to 8.5 | VKF | Tunnel-Free Oscillation |
| ▨ | 0.016 | $\approx 0.65 \times 10^6$ | 0.0026 to 0.007 | $\alpha_0 = 0.5$ to 5.5 | ARL | Tunnel-Free Oscillation (Ref. 11) |
| ⧖ | 0 | $\approx 0.56 \times 10^6$ | 0.0147 | $\alpha_0 = 1.75$ | LTV | Tunnel-Free Oscillation (Moment Reference Adjusted from 54.8 percent $\ell$) |

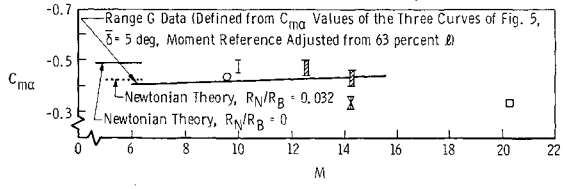


**Fig. 18 Comparison of range and tunnel $C_{m\alpha}$ data at high Mach numbers (moment reference at 60% $l$).**

Tunnel-Free Oscillation (Sting-Supported Models)

| Sym | $R_N/R_B$ | cg | $Re_\ell$ | $\omega d/2V$ | Amplitude, deg | Facility | Ref. No. |
|---|---|---|---|---|---|---|---|
| ○ | 0.016 | 60 | $\approx 0.65 \times 10^6$ | 0.0026 to 0.007 | $\alpha_0 = 0.5$ to 5.5 | ARL | 11 |
| △ | 0 | 54.8 | $\approx 0.56 \times 10^6$ | 0.0147 | $\alpha_0 = 1.75$ | LTV | |
| □ | 0 | 54.8 | $\approx 0.165 \times 10^6$ | 0.0115 | $\alpha_0 = 1.75$ | LTV | |
| ⌶ | 0.017 | 58.7 | $0.35 \times 10^6$ | 0.0024 to 0.0125 | $\alpha_{mean} = 1.5$ | VKF | 10 |
| ◇ | 0.0167 | 55 | $0.25 \times 10^6$ | 0.023 | $\alpha_{mean} = 2$ | VKF | 10 |
| ◁ | 0.017 | 58.7 | $0.28 \times 10^6$ | 0.0019 to 0.0107 | $\alpha_0 = 1.5$ | ARL | 12 |

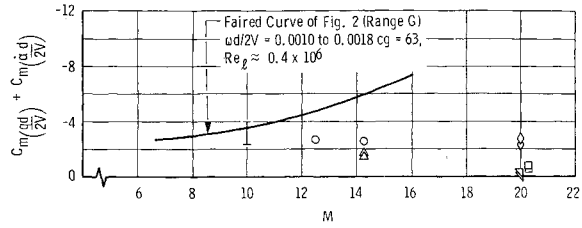


**Fig. 19 Comparison of range and tunnel damping data at high Mach numbers.**

than the range measurements; hence, the lower $C_{m\alpha}$ level indicated in the tunnel measurements at the higher Mach numbers is not understood. However, as indicated in Fig. 18, the reduced frequency parameter, $\omega d/2V$, was higher in the tests corresponding to the lower $C_{m\alpha}$ values. Further, the cause of the difference in the $C_{m\alpha}$ measurements from the different facilities at $M \approx 14.2$ is not apparent.

In Fig. 19, a comparison is made of range damping data (faired curve replotted from Fig. 2) and wind-tunnel damping data for high Mach numbers obtained from different facilities[10–12]; the tunnel tests involved sting-supported models. Again, the range free-flight damping measurements are, in general, higher than the tunnel measurements. It should be noted that $Re_l$ was similar for all data shown and that the pivot axis location in the tunnel tests was always more forward than the $cg$ position of the models involved in the range tests. There is considerable spread in the frequencies associated with tunnel tests, but there is no consistent frequency effect observed which could account for the large difference existing between the range and tunnel damping measurements.

## VI. Concluding Remarks

A free-flight range investigation of the stability and drag of a 10° semiangle cone was made at Mach numbers from 6 to 16. The measurements indicate that the damping of the cone increases appreciably with increasing Mach number between $M = 8$ and 16 at a $Re_l$ of about $0.4 \times 10^6$. Also, $C_{m\alpha}$ for the cone decreases significantly as the $R_N/R_B$ ratio is increased up to 0.1 for amplitudes greater than about 5°.

Comparisons of the range stability data with wind-tunnel data involving sting-supported models in different test facilities indicate that appreciable differences exist in the measurements. The cause of the differences in the range and tunnel stability data noted in this paper is not completely understood. It appears that tunnel support effects are one possible explanation for these differences.

## References

[1] Hobbs, R. B., Jr., "Hypersonic Dynamic Stability, Part II. Conical Body Experimental Program," FDL-TDR-64-149, Part II, Jan. 1967, Flight Dynamics Laboratory, Wright-Patterson Air Force Base, Ohio.

[2] Welsh, C. J., Winchenbach, G. L., and Madagan, A. N., "Free-Flight Investigation of the Aerodynamic Characteristics of a 10° Semi-angle Cone at Mach Numbers from 6 to 16," AEDC-TR-69-63, April 1969, Arnold Engineering Development Center, Arnold Air Force Station, Tenn.

[3] Welsh, C. J. and Watt, R. M., "Effects of Roll on the Free-Flight Motion of Statically Stable Bodies," AEDC-TR-67-156 (AD658433), Sept. 1967, Arnold Engineering Development Center, Arnold Air Force Station, Tenn.

[4] Sauerwein, H., "Application of the Piston Analogy to the Calculation of Stability Derivatives for Pointed Axially Symmetric Bodies at High Mach Numbers," RAD-TM-61-40, Oct. 1961, Avco Corporation, Wilmington, Mass.

[5] Brong, E. A., "The Unsteady Flow Field about a Right Circular Cone in Unsteady Flight," FDL-TDR-64-148, Jan. 1967, Flight Dynamics Lab., Wright-Patterson Air Force Base, Ohio.

[6] Rogers, T., Giesecke, A. H., and Hammitt, A. G., "A Fluid Ejection System for Ballistic Range Testing," AIAA Paper 68-19, New York, 1967.

[7] Clay, J. T., "Nose Bluntness, Cone Angle, and Mach Number Effects on the Stability Derivatives of Slender Cones," ARL 67-0185, Sept. 1967, Aerospace Research Labs., Wright-Patterson Air Force Base, Ohio.

[8] Rie, H., Linkiewicz, E. A., and Eosworth, F. D., "Hypersonic Dynamic Stability Part III, Unsteady Flow Field Program," FDL-TDR-64-149, Part III (AD650879), Jan. 1967, Flight Dynamics Lab., Wright-Patterson Air Force Base, Ohio.

[9] Prislin, R. H., "High-Amplitude Dynamic-Stability Characteristics of Blunt 10-Degree Cones," TR 32-1012, Oct. 1966, Jet Propulsion Lab., Pasadena, Calif.

[10] Urban, R. H., "A Dynamic Stability Balance for Hypervelocity (Hotshot) Tunnels," AEDC-TR-65-222 (AD472707), Oct. 1965, Arnold Engineering Development Center, Arnold Air Force Station, Tenn.

[11] Walchner, O. et al., "Hypersonic Stability Derivatives for a Standard 10 Degree Cone," ARL 67-0099, May 1967, Aerospace Research Labs., Wright-Patterson Air Force Base, Ohio.

[12] Urban, R. H. and Shanahan, R. J., "Dynamic Stability Characteristics of a 10-deg Cone at Mach Number 20," AEDC-TR-65-80 (AD461260), April 1965, Arnold Engineering Development Center, Arnold Air Force Station, Tenn.